ACS APPLIED MATERIALS & INTERFACES

Research Article

www.acsami.org

Prediction of Novel High-Pressure Structures of Magnesium Niobium Dihydride

Chuanzhao Zhang,[†,‡,§] Guoliang Sun,[‡] Jingjing Wang,[†] Cheng Lu,[*,‡,∥] Yuanyuan Jin,[§] Xiaoyu Kuang,[*,†] and Andreas Hermann[*,⊥]

[†]Institute of Atomic and Molecular Physics, Sichuan University, Chengdu 610065, China

[‡]Department of Physics, Nanyang Normal University, Nanyang 473061, China

[§]Department of Physics and Optoelectronic Engineering, Yangtze University, Jingzhou 434023, China

[∥]Department of Physics and High Pressure Science and Engineering Center, University of Nevada, Las Vegas, Nevada 89154, United States

[⊥]Centre for Science at Extreme Conditions and SUPA, School of Physics and Astronomy, The University of Edinburgh, Edinburgh EH93JZ, United Kingdom

Supporting Information

ABSTRACT: On the basis of a combination of the particle-swarm optimization technique and density functional theory (DFT), we explore the crystal structures of MgH_2, NbH_2, and $MgNbH_2$ under high pressure. The enthalpy−pressure (H−P) diagrams indicate that the structural transition sequence of MgH_2 is $\alpha \rightarrow \gamma \rightarrow \delta \rightarrow \varepsilon \rightarrow \zeta$ and that NbH_2 transforms from the $Fm\bar{3}m$ phase to the $Pnma$ phase at 47.80 GPa. However, $MgNbH_2$ is unstable when the pressure is too low or too high. Two novel $MgNbH_2$ structures, the hexagonal $P\bar{6}m2$ phase and the orthorhombic $Cmcm$ phase, are discovered, which are stable in the pressure ranges of 13.24−128.27 GPa and 128.27−186.77 GPa, respectively. The $P\bar{6}m2$ phase of $MgNbH_2$ consists of alternate layers of polymetric NbH_6 and MgH_6 triangular prisms, while the $Cmcm$ phase contains distorted MgH_6 trigonal prisms. The calculated elastic constants and phonon dispersions confirm that both phases are mechanically and dynamically stable. The analyses of density of states (DOS), electron localization function (ELF), and Bader charge demonstrate that a combination of ionic and metallic bonds exist in both $P\bar{6}m2$ and $Cmcm$ phases. We hope the newly predicted magnesium niobium dihydrides with desirable electronic properties will promote future experimental and theoretical studies on mixed main group-transition metal hydrides.

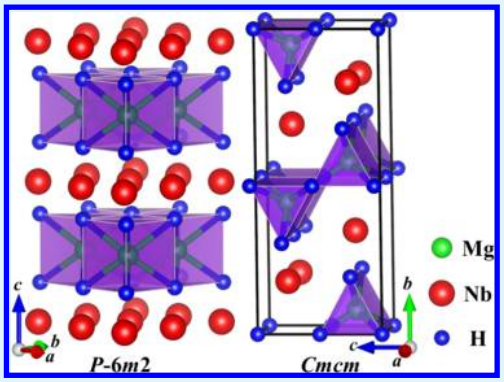

KEYWORDS: *magnesium niobium dihydride, particle swarm optimization algorithm, density functional theory, structural transition, electronic structures*

INTRODUCTION

Over the past decades, magnesium hydride (MgH_2) has been considered one of the most promising candidates for the reversible storage of hydrogen because of its low price and high weight percent storage (7.6 wt %).[1−3] Nevertheless, major shortcomings such as slow hydrogenation and dehydrogenation kinetics and the requirement of high temperatures (∼300 °C) for decomposition have significantly restricted the development of magnesium hydride in mobile applications. To solve these problems and improve the hydrogen storage properties, various attempts to add transition metals to magnesium hydride through high-pressure syntheses have been made. These attempts have been successful for the metals Nb, Ti, V, Hf, Zr, and Ta.[4−6] To date, several ternary Mg−Nb hydride compounds have been experimentally synthesized through doping MgH_2 with niobium metal and theoretically investigated using density functional theory (DFT). These include $MgNb_2H_6$, Mg_7NbH_{16}, Mg_6NbH_{16}, $Mg_{6.5}NbH_{\sim 14}$, and $MgNb_2H_{\sim 4}$.[4−6] In Figure 1, we construct the ternary Mg−Nb−H_2 phase diagram that comprises known and predicted Mg−H and Nb−H binary compounds and the ternary compounds listed above. The $MgNbH_2$ compound, so far unknown in the literature, is situated in the middle of this phase diagram. To successfully synthesize the considered $MgNbH_2$ compound under high pressure, we consider using not only MgH_2 but also NbH_2 as starting materials, as both MgH_2 and NbH_2 are stable under ambient conditions. On the basis of the synthesis routes of $MgNbH_2$, several crucial questions will arise. Can the ternary $MgNbH_2$ compound stably exist under ambient conditions? Does $MgNbH_2$ transform under pressure, and what are the structural and energetic characteristics of such transitions? How do the electronic properties of stable

Received: May 2, 2017
Accepted: July 14, 2017
Published: July 14, 2017

DOI: 10.1021/acsami.7b06143
ACS Appl. Mater. Interfaces 2017, 9, 26169−26176

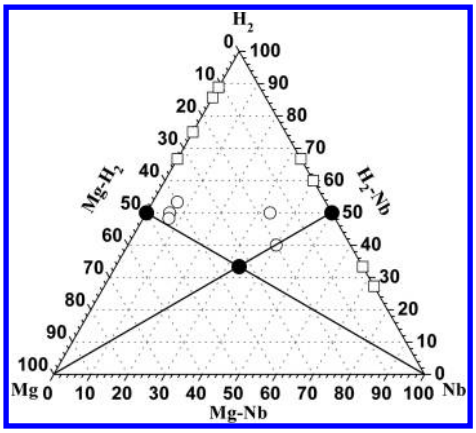

Figure 1. Ternary Mg–Nb–H_2 phase diagram. Open circles refer to experimental syntheses (see text for details); open squares refer to predicted high-pressure binary phases.[7−9] Filled circles denote MgH_2, NbH_2, and $MgNbH_2$.

$MgNbH_2$ structures change compared to both MgH_2 and NbH_2?

For the potential starting materials MgH_2 and NbH_2, extensive theoretical and experimental studies on their pressure-induced phase transformations have been carried out previously. Vajeeston et al.[10] deduced from density-functional total-energy calculations that the structural sequence of MgH_2 should be $\alpha(P4_2/mnm) \rightarrow \gamma(Pbcn) \rightarrow \beta(Pa\bar{3}) \rightarrow \delta(Pbc2_1) \rightarrow \varepsilon(Pnma)$ with respective transformation pressures of 0.39, 3.84, 6.73, and 10.26 GPa. They subsequently confirmed these theoretical results using high-pressure synchrotron X-ray diffraction.[11] However, Moriwaki et al.[12] proposed the structural sequence of MgH_2 under pressure as $\alpha \rightarrow \gamma \rightarrow \delta \rightarrow \varepsilon$, where the structural transformation process is as follows: α- and γ-MgH_2 coexist below 9 GPa. MgH_2 transforms to δ-MgH_2 above 9 GPa; it then transforms further to orthorhombic ε-MgH_2 at around 17 GPa. The energy difference between δ-MgH_2 and a competing orthorhombic phase often seen in AB_2 oxides (space group *Pbca*) is very small, and structural refinements could not distinguish between them. Subsequently, two novel high-pressure phases with space group $I4_1/amd$ and *Pnnm* were predicted.[13,14] Very recently, Lonie et al.[7] found that the ε-phase of MgH_2 slightly distorts to a higher symmetry Ni_2In-type configuration, ζ-MgH_2 ($P6_3/mmc$) at around 165 GPa. Feng et al.[9] revealed that MgH_6 is a good superconductor with a high superconducting critical temperature of ~260 K above 300 GPa. For NbH_2, Gao et al.,[8] in their computational study of the ground-state structures and properties of niobium hydrides under pressure, observed a transformation from the tetragonal $Fm\bar{3}m$ structure to an orthorhombic *Pnma* phase at about 50 GPa. They also proposed that NbH_4 should be a plausible candidate to become a superconductor with an estimated $T_c \approx 38$ K at 300 GPa. For NbH_2, a different high-pressure structure with hexagonal $P6_3mc$ symmetry was recently predicted by Chen et al. to become stable at about 45 GPa.[15] Accordingly, the phase transition sequences of MgH_2 and NbH_2 athigh pressure are still somewhat ambiguous, and reliable simulations are needed to reveal the true high-pressure behaviors of MgH_2 and NbH_2. To address the ambiguities of the phase transition processes of MgH_2 and NbH_2 and avoid similar problems for $MgNbH_2$, we need to conduct a comprehensive investigation on the structural and electronic properties of MgH_2, NbH_2, and $MgNbH_2$.

In the present work, we employed the recently developed Crystal Structure Analysis by Particle Swarm Optimization (CALYPSO) method in combination with first-principles calculations to extensively explore and search for the structures of MgH_2, NbH_2, and $MgNbH_2$ over the pressure range of 0–200 GPa. We obtain thermodynamically stable structures and identify a large number of stable phases which may be synthesized under specific pressure conditions. We examine in detail their structures, their dynamical and mechanical stability, electronic properties, and the bonding characteristics of the stable $MgNbH_2$ phases. We extend our computational investigation to pressures much higher than those used in hydrogen storage. There is much interest in the formation of hydrogen-rich metal hydrides under pressure, such as for superconductivity as seen recently in sulfur and phosphorus hydrides,[16] or the emergence of new chemistry, such as bound H_3^+ cations in H_5Cl and hydrogen cages in CaH_6.[17,18] While stable only at very high pressures, the emergence of such materials properties motivates synthesis studies at much less extreme conditions. One successful avenue pursued in high T_c cuprate and iron superconductors was to increase materials complexity, e.g., by ad-mixing different metal cations. We pursue a similar route here, in a systematic theoretical investigation of a relevant mixed metal hydride.

COMPUTATIONAL METHODS

To obtain stable structures of MgH_2, NbH_2, and $MgNbH_2$, we conducted an unbiased structure prediction based on the particle swarm optimization algorithm as implemented in the CALYPSO 3.5 package.[18−26] This method has successfully predicted the high-pressure structures of various systems.[18,21−26] The structure predictions were performed using unit cells containing up to four formula units (f.u.) and at pressures of 50, 100, 150, and 200 GPa. In every crystal search, the first generation of structures is generated randomly with some symmetry constraints and subsequent optimizations. Each generation contains 30 structures. For subsequent generations, 60% of the structures are generated from the best (lowest enthalpy) structures in the previous generation through the particle swarm optimization algorithms, while the other 40% will be generated randomly to ensure continuous diversity of the structures. We usually followed 50 generations to achieve convergence of the sampling of the low-energy minima in configurational space. Next, among the resulting 1000–1500 structures, the 50 lowest-lying structures are collected as candidates for the lowest-enthalpy structure. Those structures within 0.5 eV (usually ~20) from the lowest-lying structures are further optimized to identify the lowest-energy structure and subsequently relaxed along the entire pressure regime.

The underlying *ab initio* structural relaxations and electronic structure calculations were performed in the framework of DFT using the Perdew–Burke–Ernzerhof (PBE) exchange-correlation functional as implemented in Vienna ab Initio Simulation Package (VASP, the 5.3.5 version).[27,28] Plane-wave basis sets and the projector augmented wave (PAW) method[29] were adopted with $2p^63s^2$, $4d^45s^1$, and $1s^1$ treated as valence electron space for Mg, Nb, and H, respectively. A plane wave cutoff energy of 800 eV and appropriate Monkhorst–Pack k-meshes[30] were chosen to ensure that all the enthalpy calculations were well converged to less than 1 meV/atom. The phonon dispersion curves were computed by the direct supercell calculation method as implemented in the Phonopy program.[31,32] The electron localization function (ELF)[33,34] was also calculated using VASP. Figures of crystal structures and ELF are produced using the VESTA software.[35]

RESULTS AND DISCUSSION

MgH_2. First, based only on its chemical composition, we have implemented structure prediction simulations for MgH_2 in

DOI: 10.1021/acsami.7b06143
ACS Appl. Mater. Interfaces 2017, 9, 26169–26176

the pressure range of 0−200 GPa. A variety of structures are found to be the stable/metastable phases under specific conditions. See the Supporting Information for their lattice parameters and atomic coordinates at ambient pressure (Table S1) as well as visualizations (Figure S1). The experimental and theoretical structures were successfully reproduced, which strongly supports the validity of CALYPSO methodology used in structure searches of MgH_2. The enthalpy−pressure ($H-P$) relations of the most relevant candidate structures for MgH_2 within the pressure ranges of 0−30 and 30−200 GPa are shown in Figure 2. Under ambient pressure conditions, in the

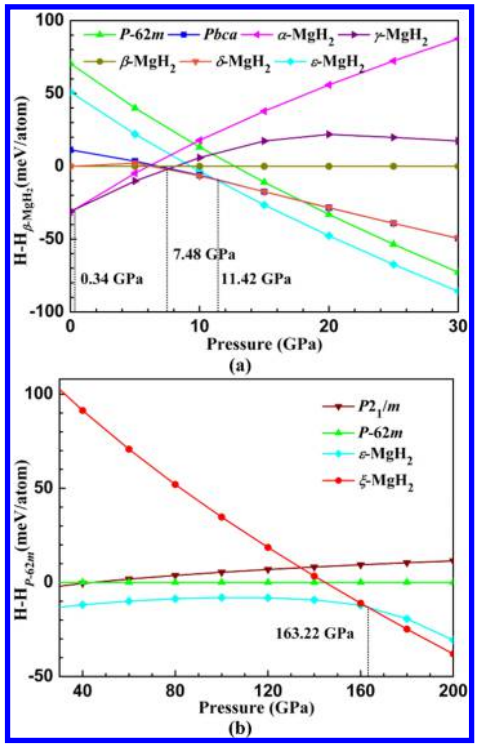

Figure 2. Enthalpies per atom in MgH_2 as functions of pressure with respect to (a) β-MgH_2 ($Pa\bar{3}$) over the pressure range of 0−30 GPa and (b) $P\bar{6}2m$ phase over the pressure range of 30−200 GPa.

ground state, we find that α-MgH_2 adopts the tetragonal $P4_2/mnm$ structure and then transforms into γ-MgH_2 at 0.34 GPa. Subsequently, γ-MgH_2 is stable over the pressure range from 0.34 to 7.48 GPa, followed by δ-MgH_2 as the most stable structure in the pressure range of 7.48−11.42 GPa. Upon further compression, δ-MgH_2 is predicted to transform into ε-MgH_2 at 11.42 GPa, which remains stable up to 163.22 GPa. These calculated transition pressures (0.34, 7.48, and 11.42 GPa) are in excellent agreement with previous computational results of 0.39, 6.73, and 10.26 GPa, respectively.[10] Beyond the last transition (>163.22 GPa), ζ-MgH_2 with a hexagonal structure is found to be energetically favorable up to at least 200 GPa, which is also in good agreement with previous calculations.[7] We also find (see Figure 2a) that the energy difference between the *Pbca* and the $Pbc2_1$ modification of δ-MgH_2 is very small, in agreement with the previous results by Vajeeston et al.[10] and Moriwaki et al.[12] We find that the $Pbc2_1$ structure is more stable than the *Pbca* structure below 14.42 GPa while the latter is more stable than the former above 14.42 GPa. Furthermore, it should be noted that we do not find β-MgH_2 to be stable at any pressure conditions; its appearance in experiment[36] could be due to finite temperature effects, which we do not consider here. From the above results, we can conclude that MgH_2 undergoes a series of structural transitions over the pressure range of 0−200 GPa, $\alpha \rightarrow \gamma \rightarrow \delta \rightarrow \varepsilon \rightarrow \zeta$, at 0.34, 7.48, 11.42, and 163.22 GPa, respectively. This structural sequence for MgH_2 in the ground state is also supported by the volume-pressure relations, as depicted in Figure S2: The four transitions are accompanied by volume reductions of 1.7, 9.0, 5.6, and 1.7%, respectively. Below, we focus on the α-MgH_2 configuration at 1 atm, the γ-MgH_2 configuration at 5 GPa, the δ-MgH_2 configuration at 10 GPa, the ε-MgH_2 configuration at 100 GPa, and the ζ-MgH_2 configuration at 180 GPa, each of which may be synthesized at the corresponding pressures. The crystal structures of these five MgH_2 phases are presented in Figure 3, and their structural parameters are shown in Table S2.

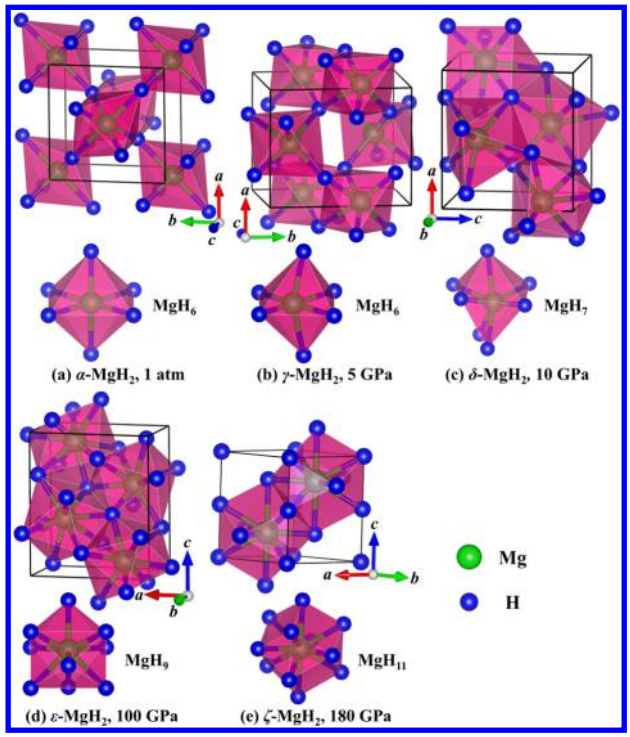

Figure 3. Crystal structures of five considered MgH_2 phases, together with metal coordination polyhedra: (a) α-MgH_2 (TiO_2-rutile type) at 1 atm, (b) γ-MgH_2 (α-PbO_2 type) at 5 GPa, (c) δ-MgH_2 ($Pbc2_1$ structure) at 10 GPa, (d) ε-MgH_2 (cotunnite-type) at 100 GPa, and (e) ζ-MgH_2 (Ni_2In type) at 180 GPa.

In α-MgH_2 at 1 atm, each Mg atom is at the center of an oblate MgH_6 octahedron: Two polar Mg−H separations are 1.939 Å, and four equatorial Mg−H separations are 1.953 Å. The smallest H−Mg−H angles are 79, 90, and 101°. These results characterize that the Mg environment in α-MgH_2 are slightly distorted octahedrons. In γ-MgH_2 at 5 GPa, one Mg atom is also surrounded by six H atoms, with the Mg−H separations varying from 1.857 to 1.950 Å and the H−Mg−H angles varying from 78 to 101°. Hence, the Mg−H atom arrangements can be considered more strongly distorted MgH_6 octahedrons. In δ-MgH_2 at 10 GPa, there are seven H atoms around each Mg. The Mg−H separations vary widely from 1.834 to 2.087 Å, and the H−Mg−H angles vary between 68 and 133°. Thus, the Mg environment in δ-MgH_2 can be described as highly distorted MgH_7 enneahedrons. In ε-MgH_2 at 100 GPa, each Mg atom is surrounded by nine H atoms with

DOI: 10.1021/acsami.7b06143
ACS Appl. Mater. Interfaces 2017, 9, 26169−26176

the Mg−H separations varying from 1.654 to 1.917 Å and the H−Mg−H angles varying between 67 and 136°. These results suggest that the Mg environment in ε-MgH_2 is best described as highly distorted MgH_9 cuboctahedrons. In ζ-MgH_2 at 180 GPa, each Mg atom is surrounded by three H atoms at a separation of 1.578 Å, two H atoms at a separation of 1.765 Å, and a further six H atoms at a separation of 1.808 Å. The Mg environment is thus best seen as an irregular dodecahedron. MgH_2 therefore undergoes, in the pressure range of 0−200 GPa, a series of structural feature transitions: MgH_6 octahedrons → MgH_7 enneahedrons → MgH_9 cuboctahedrons → MgH_{11} dodecahedrons. The coordination number of the Mg atoms in MgH_2 increase monotonously with increasing pressure. This is the main driving force for the phase transitions; upon further compression, in each of the stable MgH_2 phases we observed that the shortest Mg−H distance decrease with pressure. As presented in Figure S3, our phonon calculations verified that all five energetically relevant structures are also dynamically stable, as none of them feature imaginary phonon modes in the Brillouin zone.

To gain insight into the electronic properties of the stable MgH_2 compounds, we computed their electronic band structures and densities of states (DOS) (see Figure S4). From Figure S4, it is clear that the four stable phases of MgH_2 below 100 GPa are insulating, due to the absence of a finite electronic DOS at the Fermi level (E_F). However, ζ-MgH_2 at 180 GPa exhibits metallic character as two bands cross the Fermi level, forming an elongated hole pocket along Γ-A and electron pockets around the H point. Our calculated results suggest that metallization of MgH_2 (likely underestimated) should occur around 160−180 GPa, which is in good agreement with previous theoretical results.[37] ζ-MgH_2 becomes metallic through closure of an indirect band gap. This exciting phenomenon clearly suggests that a flat band displaying H s character rises above the Fermi level E_F around Γ-A and a steep band that boasts primarily Mg s and some Mg p character falling below E_F around the H point. The calculated band gap (from the top of the valence band to the bottom of the conduction band) for α-MgH_2 at 1 atm is 3.72 eV, which is in good agreement with the previous theoretical values of 3.4 and 4.2 eV[10,38] and less than the experimental value of 5.16 eV.[39] In fact, the present underestimation of the band gap by approximately 28% is typical for the accuracy obtained in standard DFT calculations for semiconductors and insulators. One major source of error in such calculations is the use of semilocal GGA-based exchange correlation functionals. The band gaps of the γ-, δ-, and ε-phases are calculated to be 3.78, 2.28, and 2.09 eV at 5, 10, and 100 GPa, respectively.

As displayed in the partial densities of states (PDOS) (see Figure S4), the occupied electronic states near the valence band maximum are dominated by H 1s character, while contributions from Mg 3s and Mg 2p states are limited. This means that the valence electrons of Mg are mostly transferred to the H sites and that the five MgH_2 compounds predominantly have ionic character. Relevant chemical bonding features can be identified by the ELF, as plotted in Figure S5. The ELF values of the H sites in all five MgH_2 phases are approximately equal to 1, while those of the Mg sites are extremely low. This corresponds to and confirms the DOS analysis above which shows the valence electrons have mostly transferred from the Mg to H sites. In addition, we performed a topological analysis of the charge distribution[40] for the five considered MgH_2 phases. Atom-projected partial charges are summarized in Table S3. This confirms substantial charge transfer from Mg to H atoms and further suggests that MgH_2 has primarily ionic bonding. However, the amount of charge transfer from Mg to the H atoms becomes smaller upon compression, which suggests that the iconicity of the MgH_2 compounds decreases with increasing pressure. This corroborates the closure of the band gap under pressure. In short, analyses of DOS, ELF, and Bader charges all demonstrate that the five stable MgH_2 compounds possess a dominant ionic character, which is consistent with previous results.[11]

NbH_2. Next, we performed structure predictions for NbH_2 with the CALYPSO code, in the pressure range of 0−200 GPa. All relevant predicted structures are shown in Figure S6 with their lattice parameters and atom coordinates at ambient pressure listed in Table S4. The fact that all experimental and theoretical structures were also successfully reproduced in specific pressure ranges validates our methodology as applied to NbH_2. The H−P relations of the candidate structures for NbH_2 are presented in Figure 4. At ambient pressure, the fluorite

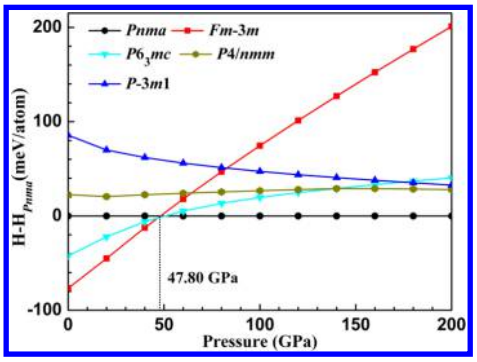

Figure 4. Enthalpy−pressure relations for NbH_2 with respect to the *Pnma* phase.

$Fm\bar{3}m$ phase has the lowest ground state energy for NbH_2, and this structure is in agreement with experimental findings.[41] With increasing pressure, the $Fm\bar{3}m$ structure transforms into an orthorhombic structure with space group *Pnma* at 47.80 GPa which remains stable in the ground state up to at least 200 GPa. This structure has been proposed in an earlier theoretical work, which predicted the $Fm\bar{3}m$ → *Pnma* transition pressure at around 50 GPa.[10] This *Pnma* structure is also the high-pressure structure of WH_2[42] and certain alkaline-earth dihydrides such as CaH_2, SrH_2, and BaH_2.[43,44] The volume−pressure relations shown in Figure S7 support the validity of the structural transition for NbH_2, as we find a volume collapse of 3.7% at the transition pressure. Below we concentrate on the properties of the $Fm\bar{3}m$ phase at 1 atm and the *Pnma* phase at 100 GPa, which are most stable and accessible to experiment at the corresponding pressures. The crystal structures for both stable NbH_2 phases are depicted in Figure 5 with their structural parameters displayed in Table S5.

In the $Fm\bar{3}m$ phase at 1 atm, each Nb atom is surrounded by eight H atoms at equal Nb−H separations of 1.982 Å. The Nb environments are regular NbH_8 cubes. In the *Pnma* phase at 100 GPa, each Nb atom is instead surrounded by nine H atoms. The Nb−H separations vary between 1.791 and 2.077 Å, and the H−Nb−H angles are in a wide range from 57 to 121°. This shows that the NbH_9 arrangements in the *Pnma* phase are highly distorted cuboctahedrons. Therefore, in a trend toward higher coordination as seen in MgH_2, the Nb−H environments

DOI: 10.1021/acsami.7b06143
ACS Appl. Mater. Interfaces 2017, 9, 26169−26176

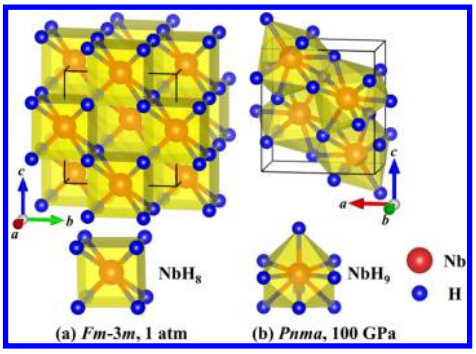

Figure 5. Crystal structures of two considered NbH_2 phases, together with NbH_n coordination environments: (a) $Fm\bar{3}m$ (fluorite) phase at 1 atm and (b) *Pnma* phase at 100 GPa.

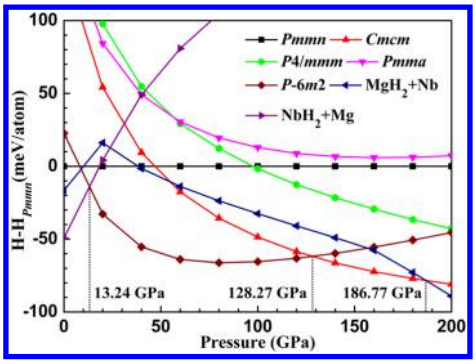

Figure 6. Enthalpy−pressure relations for $MgNbH_2$ with respect to the *Pmmn* phase.

in NbH_2 transform from NbH_8 cubes to NbH_9 cuboctahedrons as pressure increases. As shown in Figure S8, our phonon calculations verify that both structures are dynamically stable, as evidenced by the absence of any imaginary frequencies in the whole Brillouin zone.

The electronic band structures and DOS's for both stable NbH_2 phases were also computed (see Figure S9). The overlap between the conduction bands and the valence bands for these two structures suggests that they are metallic. As could be expected, the Nb 4d state contributes most to the total DOS and dominates the DOS at the Fermi level, in good agreement with findings for late transition metal hydrides.[45] To obtain a comprehensive understanding of the metallic character of both NbH_2 structures, we calculated the ELF, as plotted in Figure S10. High ELF values (approximately 1.0) are distributed around the H atoms, indicating filled $1s^2$ shells with a strongly localized character. Between the Nb and H atoms, the ELF values not only close to the Nb and H sites but also in interstitial areas are approximately 0.5, as expected for the homogeneous electron gas, while ELF near the center of the shortest Nb−H separations reduces to 0.1. Overall, ELF reflects the partially metallic and partially ionic character of the bonding in NbH_2. A Bader partial charge analysis,[40] summarized in Table S6, suggests that in the $Fm\bar{3}m$ phase at 1 atm each H atom gains approximately 0.61 *e* while the Nb atoms lose about 1.33 *e*. For the *Pnma* phase at 100 GPa, each H atom gains approximately 0.49 *e*, while the Nb atoms lose about 0.98 *e*. Even in an overall metallic state, there are large amounts of charge transfer from Nb to H atoms, revealing the ionic character of the bonding. Coupled with the DOS and ELF analyses, the bonding nature in both NbH_2 phases can be characterized as mixed metallic and ionic bonds.

$MgNbH_2$. Finally, we predict relevant structures of ternary $MgNbH_2$ using the CALYPSO method in the pressure range of 0−200 GPa. All relevant predicted structures are shown in Figure S11, and their lattice parameters and atom coordinates at ambient pressure are listed in Table S7. To investigate the two possible decomposition routes of $MgNbH_2$ (NbH_2 + Mg and MgH_2 + Nb), the H−P curves for all predicted structures together with these decompositions are shown in Figure 6 relative to our predicted *Pmmn* phase. For the elements Mg and Nb, we considered the known $P6_3/mmc$ and $Im\bar{3}m$ structures (for Mg) and $Im\bar{3}m$ and $Fm\bar{3}m$ (for Nb); see Figures S12 and S13 for their relative enthalpic behavior. The pressure evolution of $MgNbH_2$ is quite surprising. From Figure 6, we see that $MgNbH_2$ in the ground state is unstable at ambient pressure and both decomposition reactions NbH_2 + Mg and MgH_2 + Nb are exothermic. The order of stability for these three components is NbH_2 + Mg > MgH_2 + Nb > $MgNbH_2$. Stability of the decomposition product NbH_2 + Mg is found in the pressure range from 0 to 13.24 GPa. However, an intriguing hexagonal $P\bar{6}m2$ phase of $MgNbH_2$ is found to then be energetically favorable relative to NbH_2 + Mg and MgH_2 + Nb and to remain so over the wide pressure range of 13.24−128.27 GPa. Subsequently, an orthorhombic *Cmcm* structure is found as the most stable phase between 128.27 and 186.77 GPa. Above 186.77 GPa, $MgNbH_2$ again becomes unstable and is predicted to decompose into MgH_2 + Nb. Such a combination−transformation−decomposition behavior with pressure is reported here, to the best of our knowledge, for the first time in a ternary compound. The phase transition of $MgNbH_2$ at the transition pressure (128.27 GPa) results in a small volume drop of 1.4%, which is displayed in Figure S14. In view of the stability field of $MgNbH_2$ (13.24−186.77 GPa), the structural properties, mechanical and dynamical stabilities, and related electronic properties are explored in detail below for the $P\bar{6}m2$ phase at 100 GPa and the *Cmcm* phase at 160 GPa. The two newly predicted crystal structures are depicted in Figure 7

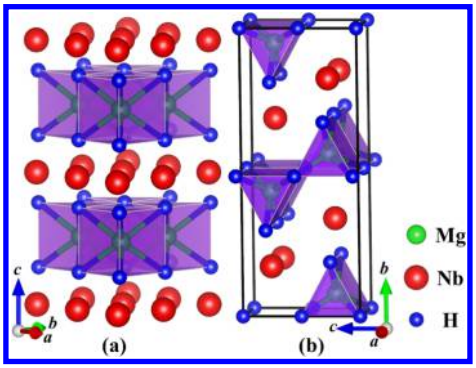

Figure 7. Crystal structures of two stable $MgNbH_2$ compounds: (a) $P\bar{6}m2$ phase at 100 GPa and (b) *Cmcm* phase at 160 GPa.

with their structural parameters presented in Table 1. As shown in Figure 7a, the $P\bar{6}m2$ structure is composed of alternate layers of polymetric NbH_6 and MgH_6 triangular prisms along the *c* axis. The Mg and Nb atoms are surrounded by six H atoms with Mg−H and Nb−H separations of 1.894 and 1.921 Å, respectively. Conversely, each H atom is surrounded by three Mg and three Nb atoms. The $P\bar{6}m2$ phase can be regarded as the NiAs structure[46] with mixed (Nb, Mg) occupancy of the Ni site and H occupancy on the As site. This structure type is similar to the *Cmcm* phase[47] of $LiBeH_3$ and the *Cmca* phase[48]

DOI: 10.1021/acsami.7b06143
ACS Appl. Mater. Interfaces 2017, 9, 26169−26176

Table 1. Structural Information of Two Stable $MgNbH_2$ Phases[a]

phase	lattice parameters (Å, °)	atom coordinates (fractional)			
		atom	*x*	*y*	*z*
$P\bar{6}m2$	*a* = 2.750, *b* = 2.750, *c* = 4.226, *γ* = 120	Mg1(1d)	0.333	0.667	0.500
		Nb1(1a)	0.000	0.000	0.000
		H1(2i)	0.667	0.333	0.744
Cmcm	*a* = 2.585, *b* = 9.358, *c* = 3.801	Mg1(4c)	0.500	0.935	0.750
		Nb1(4c)	0.000	0.174	0.750
		H1(4c)	0.000	0.812	0.750
		H2(4a)	0.000	0.000	0.500

[a] $P\bar{6}m2$ phase at 100 GPa and *Cmcm* phase at 160 GPa.

of Li_2BeH_4. In the *Cmcm* phase at 160 GPa (see Figure 7b), the Mg atoms are in a slightly distorted trigonal MgH_6 prism, with two H atoms at a separation of 1.939 Å and four H atoms at a separation of 1.953 Å. The MgH_6 trigonal prisms are aligned along the *a* axis and are edge-sharing in the *bc* plane. There are also six H atoms around each Nb atom. However, the bond lengths vary over a wide range, from 1.862 to 1.946 Å, and the H−Nb−H angles vary from 61 to 127°. Hence it is difficult to define a polyhedral Nb−H environment. The remarkable structural difference between the $P\bar{6}m2$ and *Cmcm* phases can be attributed to the pressure effect: At 160 GPa, the *Cmcm* phase is 1.2% more compact than the $P\bar{6}m2$ phase.

To verify the mechanical stability of our predicted $MgNbH_2$ structures, we calculated the elastic constants of the $P\bar{6}m2$ phase at 100 GPa and *Cmcm* phase at 160 GPa by employing the strain−stress method. The full elastic stiffness constants of both phases are given in Table S8. We find that both crystals fulfill their respective mechanical stability criteria.[49] The dynamical stability of both structures is also confirmed through the calculations of the phonon dispersion curves, as there are no imaginary phonon frequencies detected in the whole Brillouin zone; see Figures 8a,c.

The electronic properties for the $P\bar{6}m2$ phase at 100 GPa and the *Cmcm* phase at 160 GPa were investigated by analyzing their electronic band structures, total densities of states (TDOS), and PDOS; see Figure 8. Clearly, both structures exhibit metallic character as evident by the finite electronic DOS at the Fermi level (E_F). For both compounds, the TDOS near the Fermi level is largely contributed by the Nb 4d states, so the metallic properties are mainly due to partially filled Nb 4d shell. Contributions from the Mg 3s and Mg 2p states are negligible, suggesting that the valence electrons of the Mg atoms in these two structures transfer to the H atoms nearby. To obtain a more quantitative understanding of the chemical bonding in $MgNbH_2$, we conduct ELF analysis on the $P\bar{6}m2$ phase at 100 GPa and *Cmcm* phase at 160 GPa, as presented in Figure 9. In both phases, the ELF values around the Mg atoms

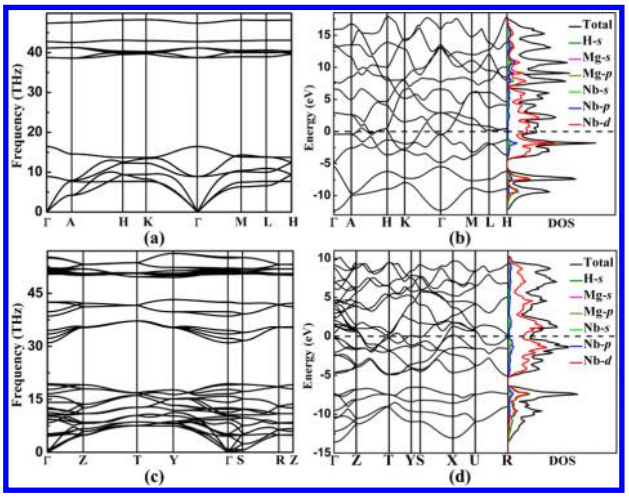

Figure 8. Phonon dispersion curves and electronic structures for two $MgNbH_2$ phases. The phonon dispersion curves for (a) $P\bar{6}m2$ phase at 100 GPa and (c) *Cmcm* phase at 160 GPa. Electronic band structures and density of states for (b) $P\bar{6}m2$ phase at 100 GPa and (d) *Cmcm* phase at 160 GPa.

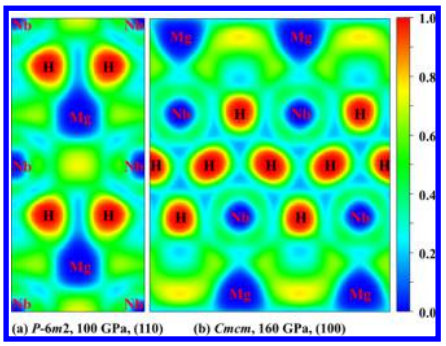

Figure 9. Electron localization function of two stable $MgNbH_2$ phases: (a) (110) plane for the $P\bar{6}m2$ phase at 100 GPa and (b) (100) plane for the *Cmcm* phase at 160 GPa.

are close 0, while the electrons near the H atoms are very localized, with ELF values close to 1.0 indicating nearly filled $1s^2$ shells. This can be explained through an Mg−H interaction that is dominantly ionic. From Figure 9, there are large interstitial areas with ELF values of about 0.5, suggesting metallic bonding feature in both compounds. A Bader charge analysis,[40] summarized in Table 2, shows that for the $P\bar{6}m2$

Table 2. Calculated Bader Charges of Mg, Nb, and H Atoms in Two Stable $MgNbH_2$ Crystals

phase	pressure (GPa)	atom	charge value (*e*)	*ω* (*e*)[a]
$P\bar{6}m2$	100	Mg	0.54	1.46
		Nb	11.05	−0.05
		H	1.71	−0.71
Cmcm	160	Mg	0.56	1.44
		Nb	11.10	−0.10
		H	1.67	−0.67

[a] *ω* is the charge transfer from Mg to a Nb or H atom.

phase at 100 GPa, a charge of 1.46 *e* is stripped off the Mg atom. The Nb atoms, on the other hand, are almost neutral (partial charge −0.05 *e*), which means almost the entire charge is transferred to the H atoms (each acquiring 0.71 *e*). At atmospheric pressure, the first ionization energy of Mg (738 kJ/mol) is higher than that of Nb (652 kJ/mol). Under pressure, it is known that higher-order angular momentum states rise slower in energy and their occupation becomes favored.[50] At 100 GPa, seemingly, the relative position of the Nb 4d states and the Mg 3s states has reversed, and ionization of the Mg valence shell is more favorable than the Nb valence states. The depopulation of the Mg valence shell is then sufficient to fill the H atom 1s shells. The same picture emerges for the *Cmcm* phase at 160 GPa: a charge of 1.44 *e* is stripped off the Mg atom

DOI: 10.1021/acsami.7b06143
ACS Appl. Mater. Interfaces 2017, 9, 26169−26176

and transferred almost entirely to the H atoms (0.67 e each), with minor charge transfer to Nb (0.10 e). The role of Nb atoms in the ternary $MgNbH_2$ is thus quite different from the hydride NbH_2, where Nb has the active role of electron donor. We thus conclude that the chemical bonding in the $P\bar{6}m2$ and $Cmcm$ phases of $MgNbH_2$ comprises a complex combination of ionic and metallic characteristics.

CONCLUSION

Using the CALYPSO method for crystal structure prediction combined with first-principles calculations, the structures of MgH_2, NbH_2, and $MgNbH_2$ within the pressure range from 0 to 200 GPa have been explored comprehensively. For MgH_2, the structural transition sequence is $\alpha \rightarrow \gamma \rightarrow \delta \rightarrow \varepsilon \rightarrow \zeta$ with transformation pressures of 0.34, 7.48, 11.42, and 163.22 GPa, respectively. For NbH_2, the $Fm\bar{3}m$ structure transforms into the orthorhombic $Pnma$ phase at 47.80 GPa. It is found that $MgNbH_2$ decomposes into NbH_2 + Mg and MgH_2 + Nb at pressures below 13.24 GPa and above 186.77 GPa, respectively. In the intermediate pressure regime, we successfully predicted two phases of $MgNbH_2$, stable with respect to NbH_2 + Mg and MgH_2 + Nb, with space groups $P\bar{6}m2$ and $Cmcm$, respectively, and an internal phase transition at 128.27 GPa. The $P\bar{6}m2$ phase, suggestively drawn with two-dimensional character in Figure 7, is composed of alternate layers of MgH_6 and NbH_6 trigonal prisms, while the $Cmcm$ structure contains distorted MgH_6 trigonal prisms. Both phases are mechanically and dynamically stable, as verified by calculating elastic constants and phonon dispersions. In both phases we find simultaneously significant ionic and metallic bonding features; the latter is stimulated by almost charge-neutral Nb atoms. This work is the first comprehensive study of mixed main group transition metal ternary hydride formation under pressure, and the method used here is expected to be applicable to exploring the pressure-induced formation of other ternary metal hydrides. The predicted onset of stability for $MgNbH_2$ should be accessible to X-ray and even neutron diffraction experiments, and the formation of a layered subhydride of 1:1 Mg/Nb would be an intriguing addition to an already quite complex phase diagram.

ASSOCIATED CONTENT

Supporting Information

The Supporting Information is available free of charge on the ACS Publications website at DOI: 10.1021/acsami.7b06143.

Details of crystal structures, volume-pressure relations and electronic properties for MgH_2, NbH_2, and $MgNbH_2$ (PDF)

AUTHOR INFORMATION

Corresponding Authors

*E-mail: lucheng@calypso.cn.
*E-mail: scu_kuang@163.com.
*E-mail: a.hermann@ed.ac.uk.

ORCID

Chuanzhao Zhang: 0000-0003-1267-2245
Cheng Lu: 0000-0003-1746-7697
Xiaoyu Kuang: 0000-0001-7489-9715

Notes

The authors declare no competing financial interest.

ACKNOWLEDGMENTS

This work was supported by the National Natural Science Foundation of China (No. 11574220, 11274235, 11304167, and 21671114), Program for Science & Technology Innovation Talents in Universities of Henan Province (No. 15HASTIT020), and Special Program for Applied Research on Super Computation of the NSFC-Guangdong Joint Fund (the second phase) (No. U1501501). Calculations were performed using the Cherry Creek Supercomputer of the UNLV's National Supercomputing Institute, as well as the National Supercomputer Center in Guangzhou.

REFERENCES

(1) Schlapbach, L.; Züttel, A. Hydrogen-Storage Materials for Mobile Applications. *Nature* **2001**, *414*, 353−358.
(2) Liu, G.; Wang, Y.; Jiao, L.; Yuan, H. Understanding the Role of Few-Layer Graphene Nanosheets in Enhancing the Hydrogen Sorption Kinetics of Magnesium Hydride. *ACS Appl. Mater. Interfaces* **2014**, *6*, 11038−11046.
(3) Zheng, S.; Li, Z. P.; Bendersky, L. A. Understanding the Role of Vanadium in Enhancing the Low-Temperature Hydrogenation Kinetics of an Mg Thin Film. *ACS Appl. Mater. Interfaces* **2013**, *5*, 6968−6974.
(4) Dong, H.; Huang, C.; Moser, D.; Noréus, D.; Zhu, M. Structure and Stability of High Pressure Synthesized $MgTM_2H_6$ (TM = Zr, Nb) Hydrides. *Acta Mater.* **2015**, *96*, 237−248.
(5) Shelyapina, M. G.; Fruchart, D.; Wolfers, P. Electronic Structure and Stability of New FCC Magnesium Hydrides Mg_7MH_{16} and Mg_6MH_{16} (M = Ti, V, Nb): An ab initio Study. *Int. J. Hydrogen Energy* **2010**, *35*, 2025−2032.
(6) Sato, T.; Kyoi, D.; Rönnebro, E.; Kitamura, N.; Sakai, T.; Noréus, D. Structural Investigations of Two New Ternary Magnesium-Niobium Hydrides, $Mg_{6.5}NbH_{\sim 14}$ and $MgNb_2H_{\sim 4}$. *J. Alloys Compd.* **2006**, *417*, 230−234.
(7) Lonie, D. C.; Hooper, J.; Altintas, B.; Zurek, E. Metallization of Magnesium Polyhydrides under Pressure. *Phys. Rev. B: Condens. Matter Mater. Phys.* **2013**, *87*, 054107.
(8) Gao, G.; Hoffmann, R.; Ashcroft, N. W.; Liu, H.; Bergara, A.; Ma, Y. Theoretical Study of the Ground-state Structures and Properties of Niobium Hydrides under Pressure. *Phys. Rev. B: Condens. Matter Mater. Phys.* **2013**, *88*, 184104.
(9) Feng, X.; Zhang, J.; Gao, G.; Liu, H.; Wang, H. Compressed Sodalite-Like MgH_6 as a Potential Hightemperature Superconductor. *RSC Adv.* **2015**, *5*, 59292−59296.
(10) Vajeeston, P.; Ravindran, P.; Kjekshus, A.; Fjellvåg, H. Pressure-Induced Structural Transitions in MgH_2. *Phys. Rev. Lett.* **2002**, *89*, 175506.
(11) Vajeeston, P.; Ravindran, P.; Hauback, B. C.; Fjellvåg, H.; Kjekshus, A.; Furuseth, S.; Hanfland, M. Structural Stability and Pressure-Induced Phase Transitions in MgH_2. *Phys. Rev. B: Condens. Matter Mater. Phys.* **2006**, *73*, 224102.
(12) Moriwaki, T.; Akahama, Y.; Kawamura, H.; Nakano, S.; Takemura, K. Structural Phase Transition of Rutile-Type MgH_2 at High Pressures. *J. Phys. Soc. Jpn.* **2006**, *75*, 074603.
(13) Song, Y.; Guo, Z. X. Metastable MgH_2 Phase Predicted by First Principles Calculations. *Appl. Phys. Lett.* **2006**, *89*, 111911.
(14) Zhang, L.; Wang, Y.; Cui, T.; Li, Y.; Li, Y.; He, Z.; Ma, Y.; Zou, G. $CaCl_2$-type High-pressure Phase of Magnesium Hydride Predicted by ab initio Phonon Calculations. *Phys. Rev. B: Condens. Matter Mater. Phys.* **2007**, *75*, 144109.
(15) Chen, C.; Tian, F.; Duan, D.; Bao, K.; Jin, X.; Liu, B.; Cui, T. Pressure Induced Phase Transition in MH_2 (M = V, Nb). *J. Chem. Phys.* **2014**, *140*, 114703.
(16) Drozdov, A. P.; Eremets, M. I.; Troyan, I. A.; Ksenofontov, V.; Shylin, S. I. Conventional Superconductivity at 203 K at High Pressures in the Sulfur Hydride System. *Nature* **2015**, *525*, 73−76.

(17) Wang, Z.; Wang, H.; Tse, J. S.; Iitaka, T.; Ma, Y. Stabilization of H_3^+ in the High Pressure Crystalline Structure of $H_nCl(n = 2–7)$. *Chem. Sci.* **2015**, *6*, 522–526.
(18) Wang, H.; Tse, J. S.; Tanaka, K.; Iitaka, T.; Ma, Y. Superconductive Sodalite-Like Clathrate Calcium Hydride at High Pressures. *Proc. Natl. Acad. Sci. U. S. A.* **2012**, *109*, 6463–6466.
(19) Wang, Y.; Lv, J.; Zhu, L.; Ma, Y. Crystal Structure Prediction via Particle-swarm Optimization. *Phys. Rev. B: Condens. Matter Mater. Phys.* **2010**, *82*, 094116.
(20) Wang, Y.; Lv, J.; Zhu, L.; Ma, Y. CALYPSO: A Method for Crystal Structure Prediction. *Comput. Phys. Commun.* **2012**, *183*, 2063–2070.
(21) Lv, J.; Wang, Y.; Zhu, L.; Ma, Y. Predicted Novel High-Pressure Phases of Lithium. *Phys. Rev. Lett.* **2011**, *106*, 015503.
(22) Zhu, L.; Liu, H.; Pickard, C. J.; Zou, G.; Ma, Y. Reactions of Xenon with Iron and Nickel are Predicted in the Earth's Inner Core. *Nat. Chem.* **2014**, *6*, 644–648.
(23) Zhu, L.; Wang, H.; Wang, Y.; Lv, J.; Ma, Y.; Cui, T.; Ma, Y.; Zou, G. Substitutional Alloy of Bi and Te at High Pressure. *Phys. Rev. Lett.* **2011**, *106*, 145501.
(24) Li, Y.; Hao, J.; Liu, H.; Li, Y.; Ma, Y. The Metallization and Superconductivity of Dense Hydrogen Sulfide. *J. Chem. Phys.* **2014**, *140*, 174712.
(25) Liu, H.; Naumov, I. I.; Hemley, R. J. Dense Hydrocarbon Structures at Megabar Pressures. *J. Phys. Chem. Lett.* **2016**, *7*, 4218–4222.
(26) Yong, X.; Liu, H.; Wu, M.; Yao, Y.; Tse, J. S.; Dias, R.; Yoo, C. S. Crystal Structures and Dynamical Properties of Dense CO_2. *Proc. Natl. Acad. Sci. U. S. A.* **2016**, *113*, 11110–11115.
(27) Kresse, G.; Furthmüller, J. Efficient Iterative Schemes for ab initio Total-Energy Calculations Using a Plane-Wave Basis Set. *Phys. Rev. B: Condens. Matter Mater. Phys.* **1996**, *54*, 11169–11186.
(28) Perdew, J. P.; Burke, K.; Ernzerhof, M. Generalized Gradient Approximation Made Simple. *Phys. Rev. Lett.* **1996**, *77*, 3865–3868.
(29) Kresse, G.; Joubert, D. From Ultrasoft Pseudopotentials to the Projector Augmented-Wave Method. *Phys. Rev. B: Condens. Matter Mater. Phys.* **1999**, *59*, 1758–1775.
(30) Monkhorst, H. J.; Pack, J. D. Special Points for Brillouin-zone Integrations. *Phys. Rev. B* **1976**, *13*, 5188–5192.
(31) Parlinski, K.; Li, Z. Q.; Kawazoe, Y. First-Principles Determination of the Soft Mode in Cubic ZrO_2. *Phys. Rev. Lett.* **1997**, *78*, 4063–4066.
(32) Togo, A.; Oba, F.; Tanaka, I. First-principles Calculations of the Ferroelastic Transition between Rutile-type and $CaCl_2$-type SiO_2 at High Pressures. *Phys. Rev. B: Condens. Matter Mater. Phys.* **2008**, *78*, 134106.
(33) Becke, A. D.; Edgecombe, K. E. A Simple Measure of Electron Localization in Atomic and Molecular Systems. *J. Chem. Phys.* **1990**, *92*, 5397–5403.
(34) Savin, A.; Jepsen, O.; Flad, J.; Andersen, O. K.; Preuss, H.; von Schnering, H. G. Electron Localization in Solid-state Structures of the Elements: the Diamond Structure. *Angew. Chem., Int. Ed. Engl.* **1992**, *31*, 187–188.
(35) Momma, K.; Izumi, F. VESTA 3 for Three-Dimensional Visualization of Crystal, Volumetric and Morphology Data. *J. Appl. Crystallogr.* **2011**, *44*, 1272–1276.
(36) Bastide, J. P.; Bonnetot, B.; Létoffé, J. M.; Claudy, P. Polymorphisme de L'hydrure de Magnesium Sous Haute Pression. *Mater. Res. Bull.* **1980**, *15*, 1779–1787.
(37) Zhang, C.; Chen, X. J.; Zhang, R. Q.; Lin, H. Q. Chemical Trend of Pressure-Induced Metallization in Alkaline Earth Hydrides. *J. Phys. Chem. C* **2010**, *114*, 14614–14617.
(38) Pfrommer, B.; Elsässer, C.; Fähnle, M. Possibility of Li-Mg and Al-Mg Hydrides Being Metallic. *Phys. Rev. B: Condens. Matter Mater. Phys.* **1994**, *50*, 5089–5093.
(39) Yu, R.; Lam, P. K. Electronic and Structural Properties of MgH_2. *Phys. Rev. B: Condens. Matter Mater. Phys.* **1988**, *37*, 8730–8737.
(40) Bader, R. F. *Atoms in Molecules: A Quantum Theory*; Clarendon Press: Oxford, 1994.
(41) Reilly, J. J.; Wiswall, R. H. The higher Hydrides of Vanadium and Niobium. *Inorg. Chem.* **1970**, *9*, 1678–1682.
(42) Scheler, T.; Peng, F.; Guillaume, C. L.; Howie, R. T.; Ma, Y.; Gregoryanz, E. Nanocrystalline Tungsten Hydrides at High Pressures. *Phys. Rev. B: Condens. Matter Mater. Phys.* **2013**, *87*, 184117.
(43) Li, Y.; Li, B.; Cui, T.; Li, Y.; Zhang, L.; Ma, Y.; Zou, G. High-Pressure Phase Transformations in CaH_2. *J. Phys.: Condens. Matter* **2008**, *20*, 045211.
(44) El Gridani, A. H.; El Bouzaidi, R. D.; El Mouhtadi, M. Elastic, Electronic and Crystal Structure of BaH_2: A Pseudopotential Study. *J. Mol. Struct.: THEOCHEM* **2002**, *577*, 161–175.
(45) Gao, G.; Wang, H.; Zhu, L.; Ma, Y. Pressure-Induced Formation of Noble Metal Hydrides. *J. Phys. Chem. C* **2012**, *116*, 1995–2000.
(46) Yao, Y.; Klug, D. D. High-Pressure Phases of Lithium Borohydride $LiBH_4$: A First-Principles Study. *Phys. Rev. B: Condens. Matter Mater. Phys.* **2012**, *86*, 064107.
(47) Hu, C. H.; Oganov, A. R.; Lyakhov, A. O.; Zhou, H. Y.; Hafner, J. Insulating States of $LiBeH_3$ under Extreme Compression. *Phys. Rev. B: Condens. Matter Mater. Phys.* **2009**, *79*, 134116.
(48) Wang, H.; Li, Q.; Wang, Y.; Gao, G.; Ma, Y. High-Pressure Polymorphs of Li_2BeH_4 Predicted by First-Principles Calculations. *J. Phys.: Condens. Matter* **2009**, *21*, 385405.
(49) Wu, Z.; Zhao, E.; Xiang, H.; Hao, X.; Liu, X.; Meng, J. Crystal Structures and Elastic Properties of Superhard IrN_2 and IrN_3 from First Principles. *Phys. Rev. B: Condens. Matter Mater. Phys.* **2007**, *76*, 054115.
(50) Miao, M. S.; Hoffmann, R. High Pressure Electrides: A Predictive Chemical and Physical Theory. *Acc. Chem. Res.* **2014**, *47*, 1311–1317.

DOI: 10.1021/acsami.7b06143
ACS Appl. Mater. Interfaces 2017, 9, 26169–26176